Three-dimensional architecture of hair-cell linkages as revealed by electron-microscopic tomography

Manfred Auer, Bram Koster, Ulrike Ziese, Chandajit Bajaj, Niels Volkmann,

Da Neng Wang, and A. J. Hudspeth

Howard Hughes Medical Institute and Laboratory of Sensory Neuroscience,

The Rockefeller University, 1230 York Avenue, New York, NY 10021-6399

Abbreviated title:	Hair-cell linkages
Number of manuscript pages:	30
Number of figures:	11
Number of tables:	1
Number of words in Abstract (250 maximum):	134
Number of words in Introduction (500 maximum):	488
Number of words in Discussion (1500 maximum):	1491

Proofs and correspondence to:

Dr. A. J. Hudspeth

Howard Hughes Medical Institute and

Laboratory of Sensory Neuroscience

Box 314

The Rockefeller University

1230 York Avenue

New York   NY   10021-6399

Telephone: 212 / 327-7351

Facsimile: 212 / 327-7352

E-mail: hudspaj@rockefeller.edu

Key words: ankle link, auditory system, basal link, kinociliary link, kinocilium, stereocilium, tip link, vestibular system

The senses of hearing and balance rest upon mechanoelectrical transduction by the hair bundles of hair cells in the inner ear. Located at the apical cellular surface, each hair bundle comprises several tens of stereocilia and a single kinocilium that are interconnected by extracellular proteinaceous links. Using electron-microsopic tomography of bullfrog saccular sensory epithelia, we examined the three-dimensional structures of ankle or basal links, kinociliary links, and tip links. We observed clear differences in the dimensions and appearances of the three links. We found two distinct populations of tip links suggestive of the involvement of two proteins or splice variants. We noted auxiliary links connecting the upper portions of tip links to the taller stereocilia. Tip links and auxiliary links show a tendency to adopt a globular conformation when disconnected from the membrane surface.

INTRODUCTION

The fundamental role of the hair cell, the sensory receptor of the ear and lateral-line system, is that of mechanoreception. Key to the hair cell's operation are the filamentous extracellular connections between the processes of the mechanoreceptive hair bundle, of which three types occur in most instances.

First, the hexagonal arrangement of stereocilia is stabilized by links between them along all three axes (Bäggar-Sjöback, 1974; Csukas et al., 1987). Because these links impinge upon each stereocilium at the base of its cylindrical shaft, just above its basal taper, they are termed basal links. Although these connections are dispensible for mechanotransduction (Jacobs and Hudspeth, 1990), they are required for hair-bundle survival (Frolenkov et al., 2004). Similar connections, termed ankle links, occur transiently during the development of mammalian cochlear hair cells. Among several proteins whose deficiency produces Usher Syndrome, two might constitute the ankle links: cadherin 23 (Di Palma et al., 2001; Boeda et al., 2002; Siemens et al., 2002) and the very large G-protein coupled receptor, Vlgr1b (Goodyear et al., 2006).

In most receptor organs of the inner ear and lateral-line system, mechanical stimuli representing sounds, accelerations, or water movements are initially conveyed to the kinocilium by an extracellular accessory structure. Connections of a second type, kinociliary links, then transmit these stimuli to the five longest stereocilia (Hillman and Lewis, 1971). Kinociliary links constitute an array of several dozen fine strands that Fourier analysis suggests are arranged in a coiled-coil conformation (Csukas et al., 1987; Tsuprun et al., 2004).

Finally, tip links run obliquely from the ends of stereocilia to the sides of the longest adjacent stereocilia (Pickles et al., 1984). These filaments are probably connected to mechanically sensitive channels, and are therefore essential to mechanoelectrical transduction. If exposed to lanthanoid ions or Ca^{2+} chelators, tip links disappear concomitantly with the loss of responsiveness; as they regenerate over several hours, transduction recovers (Zhao et al., 1996). When analyzed by high-resolution scanning electron microscopy, each tip link appears to comprise two filaments arranged in a right-handed, coiled-coil configuration (Kachar et al., 2000). Fourier analysis of projection images suggests instead a triple-helical structure (Tsuprun and Santi, 2000). A tip link may branch 10-50 nm below its upper insertion and may contact the membrane at two or three sites at its lower end (Furness and Hackney, 1985; Kachar et al., 2000). Tip links likely consist of glycosylated protein, for polycationic compounds label them (Neugebauer and Thurm, 1987; Tsuprun and Santi, 2000) and they are severed by proteases only after deglycosylation (Kachar et al., 2000). Although cadherin 23 has been proposed on the basis of genetic and immunological evidence to occur in tip links (Siemens et al., 2004; Sollner et al., 2004), other results are conflicting (Lagziel et al., 2005; Michel et al., 2005; Rzadzinska et al., 2005).

To gain further insight into the molecular structures of the three classes of links, we conducted electron-microscopic tomography on hair bundles from the frog's sacculus.

MATERIALS AND METHODS

Sample preparation. Bullfrogs were sacrificed and the saccular maculae were dissected into oxygenated standard saline consisting of 110 mM Na^+, 2 mM K^+, 4 mM Ca^{2+}, 118 mM Cl^-, 3 mM **D**-glucose, and 5 mM HEPES at pH 7.3. Three different sample-

preparation procedures were employed for this study. The principal differences were whether a detergent was used for controlled extraction prior to fixation and whether samples were dehydrated on ice or by the method of progressive lowering of temperature (Armbruster et al. 1982; Carlemalm et al. 1982).

In the case of detergent extraction, the sensory epithelia were exposed prior to fixation for 20 min on ice to 1% Triton X-100 in a solution containing 100 mM KCl, 5 mM $MgCl_2$, 5 mM EGTA, and protease inhibitors. The preparations were then rinsed three times for 2 min each in the solution without detergent.

Sensory epithelia were fixed for 2 hrs at room temperature in 3% glutaraldehyde, 0.2% tannic acid, 100 mM KCl, 5 mM $MgCl_2$, and 20 mM MOPS at pH 6.8, then rinsed three times for 5 min each at room temperature in the same solution without the glutaraldehyde and tannic acid. After three additional rinses at 4°C, samples were incubated on ice in 1% OsO_4, 10 mM $MgCl_2$, and 100 mM K_2HPO_4/NaH_2PO_4 at pH 6.1. After three additional rinses of 5 min each in distilled water at 4°C, the maculae were stained overnight at 4°C in aqueous 1% uranyl acetate (Taylor et al., 1999).

Conventional dehydration was conducted with ethanol concentrations of 30%, 50%, 70%, 95%, and three rounds of 100% on ice for 5 min each. For dehydration with progressive lowering of temperature, each incubation period was 20 min, with exposure to 30% ethanol at 4°C, to 50% ethanol at -20°C, and to 70%, 95%, and 100% ethanol at -35°C. The tissue was allowed to warm to room temperature in 100% ethanol before embedding in an Epon-Araldite mixture.

After heat polymerization in a vacuum oven for 3 days, initially at 60°C and subsequently at 85°C, sections were cut at thicknesses of 100-120 nm, placed on 100 x 400-mesh slot grids or 200-mesh hexagonal grids, decorated with gold fiducial markers, and coated with a thin layer of carbon.

Data collection and analysis. Sections were imaged on a Philips CM200, CM200FEG, or EM430 transmission electron microscope. Tilt series were recorded at 1° intervals for angles of up to ±75° (Table 1). Projections were aligned and reconstructed into a three-dimensional volume with the software package EM3D (Harlow et al 2001), PRIISM (Chen et al., 1996), or IMOD (Kremer et al. 1996).

RESULTS

Improved preservation through low-temperature sample processing

We initially prepared specimens by conventional techniques conducted at room temperature. Because the preservation of actin filaments by these means was mediocre, we tried several variant procedures. Preservation was enhanced by carrying out the osmium tetroxide postfixation, uranyl acetate staining, and ethanol dehydration steps on ice, and by omitting a propylene oxide step altogether. The best results were obtained by dehydration during progressive lowering of temperature (Carlemalm et al. 1982; Armbruster et al. 1982).

Three-dimensional tomographic analysis of hair-bundle links

We recorded 15 tomographic data sets and conducted reconstructions at voxel sizes ranging from 0.54 nm to 1.74 nm, with most of the data analyzed at a voxel size of 0.82 nm (Table 1). We deliberately oversampled the data to reduce the risk of substantial distortion of subcellular features during the post-processing steps of filtering and segmentation.

For interactive exploration of the three-dimensional volumes, we routinely used the Volume Rover package (Bajaj et al., 2003), typically followed by one round of bilateral filtering (Jiang et al., 2003) or denoising by non-linear anisotropic diffusion

(Frangakis and Hegerl, 2001). In some cases, features were extracted by the boundary-segmentation approach (Bajaj et al., 2003) or the watershed-immersion algorithm (Volkmann, 2002). In other instances, bilaterally filtered or unfiltered data were used for interactive segmentation and model building with the Volume Path Tracer and Zone tools in Chimera (Pettersen et al., 2004). Interactive manual 3D-segmentation required the subjective choice of contour levels; we usually selected the highest threshold that nevertheless ensured connectivity of the features. Depending on the exact contour level chosen, the estimates of filament length and intermembrane distance changed by no more than 3-5 nm. Length and volume measurements were also conducted with Chimera using the Pick Surface Pieces tool. At a chosen contour level, we could determine filament lengths with an accuracy estimated at 2 nm.

Basal links

We collected two data sets of basal links from hair cells whose membranes had been detergent-treated for reasons unrelated to the present study. The membrane-to-membrane distance spanned by the links ranged in both data sets from 80 nm to 200 nm (Figure 1). Upon tracing 21 basal links in three dimensions, we found lengths ranging from 100 nm to 250 nm (Figure 2). Most filaments did not span the intermembrane distance in the shortest way possible, but were curved or S-shaped and inserted on the stereociliary membranes at an angle of 60°-80°. Filaments of differing length could readily be distinguished in a slice of the reconstructed volume (Figure 1). Although the voxel volume was limited to 1.74 nm, we estimate that length measurements were accurate within 5 nm.

Reconstruction of 11 representative basal links showed considerable heterogeneity in their structure (Figure 3). The length distribution of the filaments

suggested at least two different classes of filament, one approximately 140 nm in length and a second around 250 nm long (Figure 4*A*). The shortest links appear to consist of straight, single filaments 100-110 nm in length. Other links seem to consist of single filaments or dimers that are joined either end-to-end or side-by-side. Depending on their thickness, we interpreted the 250-nm-long filaments as either dimers or tetramers. In the instance of the putative tetramers, *en face* views revealed a doubling of the width of the density compared to other basal link filaments, suggesting a side-by-side arrangement of two filaments. The maximal number of filaments in intimate lateral contact with one another appeared to be fourother filaments seem to consist of single filaments or dimers that are joined either end-to-end or side-by-side. It therefore appears that multiple proteins displaying at least two different lengths are involved in basal links.

Kinociliary links

Three-dimensional reconstruction of a 100-nm section revealed at least three clusters of kinociliary links separated along the length of the kinocilium (Figure 5). We traced 77 kinociliary links, of which 61 spanned the entire distance between the membranes; the remainder left the volume under study or terminated on other links. The shortest distance between membranes of the tallest stereocilium and its neighboring kinocilium varied from 120 nm at the proximal end to 95 nm at the distal end of the kinociliary bulb. Although in projection views along the direction of the electron beam the links may appear as double or triple filaments twisted around each other (Tsuprun et al., 2004), three-dimensional analysis showed that the filaments are separated. Filaments appear to be grouped and insert into only the thicker membrane portions of the kinociliary bulb (Figure 5). No strict correlation was observed between link length and intermembrane

distance; instead, the links were arranged either perpendicular to the membrane or tilted, depending on the intermembrane distance to be spanned.

Kinociliary links ranged in length from 110 nm to 133 nm (Figure 4*B*). Although most appeared to be straight, some links were slightly bent or S-shaped, occasionally even displaying kinks (Figures 6 and 7). The apparent thickness of the filaments depended on the contour level selected for surface rendering; we estimate their diameter at 4 nm.

Tip links

We visualized a total of 12 tip links by electron-microscopic tomography. Eight of these were intact, with the remaining four disconnected at their basal ends (Figure 8 and 9). Although some links appeared as two filaments helically wound around each other, others displayed a sheet-like architecture consistent with two filaments lying side-by-side (Figure 9). Tip links fell into two classes, either 110-120 nm or 170 nm long (Figure 4*C*). The tip link that appeared to be best preserved accorded with a coiled-coil model in which each filament comprised two segments (Figure 10), with the upper portion containing a longer filament (93 nm) than the lower portion (70 nm). A tip link's angle of insertion at the upper stereociliary surface was typically 28°-37° and did not depend on the link's length (Table 1).

In at least six of 12 data sets, an additional extracellular density occurred at or above the insertion of the tip link on the taller stereocilium (Figure 8). Although these structures appeared amorphous in projection views, three-dimensional visualization resolved them as curled filaments (Figure 11). We also encountered one instance of two auxiliary links running from the middle of the main link towards the membrane of the taller stereocilium (Figure 11). At least one of the two links was anchored into the

stereociliary surface by a receptor molecule 20 nm in length. The auxiliary filament contacted the membrane surface 55-60 nm from its main link's attachment site, then turned 90˚ and ran perpendicular to the stereociliary axis and parallel to the membrane surface above the main link, where together with the second auxiliary link it formed the lower portion of a bi-lobed feature. The upper and lower lobes connected at their distal ends; the upper lobe appeared to be larger than the lower.

DISCUSSION

Improved sample preservation

The low probability of finding tip links and the limited success associated with cutting frozen-hydrated sections precluded cryo-electron microscopy in the present study. The contrast in our specimens therefore stemmed from the stain surrounding and penetrating proteins rather than from the proteins themselves. However, comparison of the electron density for actin filaments in our specimens with an atomic model derived from X-ray crystallography and cryo-electron microscopy supports the validity of molecular interpretations of our tomograms. Moreover, metal-stained, resin-embedded tissue has been successfully interpreted at the molecular level for acto-myosin complexes in insect flight muscle (Taylor et al., 1999) and for desmosomes (He et al., 2003). Repeated attempts of high-pressure freezing of sensory epithelia were unsuccessful in preserving the hair bundle architecture (see supplemental online material).

Although we encountered some wrinkling of stereociliary membranes, dehydration during progressive lowering of temperature resulted in generally good preservation, most clearly visible in the stereociliary cytoskeleton (Small, 1981). Because the spacing of actin filaments in stereocilia accords with that measured by cryo-

electron microscopy of filaments cross-linked by fimbrin (Volkmann et al., 2001), the stereocilia probably did not shrink significantly during preparation (Luther et al., 1988; Braunfeld et al., 1994) and hence differences in filament length cannot be attributed to shrinkage.

Organization of basal links

Because basal links are S-shaped or smoothly curved and do not span the extracellular space directly, they evidently have a somewhat rigid structure. The density maps for long basal-link filaments are best matched by a tetramer, such as a cadherin (Shapiro et al., 1995; Nagar et al., 1996), comprising two dimers arranged side-by-side and joined head-to-head. Our data are compatible with a tetramer of cadherin 23, which extends 125 nm for a model including 27 ectodomains. However, the short isoform of usherin, also predicted to be 125 nm in length (Adato et al., 2005; van Wijk et al., 2006), would be an equally good candidate. By contrast, the extracellular portion of Vlgr1b spans 180 nm (McMillan and White, 2004), a distance inconsistent with the lengths of most basal links.

Organization of kinociliary links

Unlike basal links, kinociliary links are typically oriented orthogonal to membrane surfaces. Their variation in length from 100 nm to 135 nm suggests the involvement of more than a single protein. Although we cannot exclude a contribution of cadherin 23 to the kinociliary links, the majority of the filaments analyzed by tomography are shorter than expected for a cadherin 23 monomer bound to a surface receptor. The identity of the kinociliary link therefore remains uncertain.

Organization of tip links

The striking dichotomy that we observed in the lengths of tip links is also apparent in published images (Zhao et al., 1996; Sollner et al., 2004). Variations in tip-link dimensions cannot be attributed to tissue shrinkage, for in some instances long and short links coexist in the same hair bundle. We therefore believe that such differences reflect differences in protein identity, splice isoform, or conformation.

The curled appearance of detached tip links suggests that these structures are not flexurally rigid. Our results do not bear on the extensibility of the links, and thus on their possible contribution to the stiffness of the gating springs for mechanoelectrical transduction.

In the best-preserved samples, we found evidence for an auxiliary link that originates from the main tip link. The auxiliary link appears to be anchored by a protruding density to the taller stereocilium's membrane adjacent to the main link's insertion. Although it is unclear whether the auxiliary link and main tip link are made of the same proteins, both structures occupy comparable volumes and curl up when detached. The divergence of an auxiliary link from the main tip link may underlie the forking of tip links (Furness and Hackney, 1985; Kachar et al., 2000). In our projection images, as well as in published micrographs (Zhao et al., 1996; Siemens et al., 2004), the sides of stereocilia often display globular extracellular densities that may reflect detached auxiliary links.

Candidate proteins for the tip link

Although both ultrastructural analysis of zebrafish*sputnik* mutants and immunocytochemical data suggest that cadherin 23 forms the tip link, this conclusion is controversial. Cadherin 23 nonsense mutants can nonetheless display links 100 nm in

length (Sollner et al., 2004), whereas *te370e* mutants with a four-amino-acid insertion lack tip links, but exhibit microphonic potentials and only mildly disheveled hair bundles. Mutants with a premature stop codon display a variety of phenotypes, not simply the absence of mechanotransduction that one might expect for tip links unable to anchor. Immunolabeling studies with an antibody raised against the intracellular C-terminal domain are also puzzling. Although it lacks the relevant epitope, the *t23576* mutant nevertheless displays immunolabeling (Siemens et al., 2004; Sollner et al., 2004). Electron-microscopic immunolabeling of frog sensory epithelia shows up to 12 gold particles decorating two presumed epitopes (Siemens et al., 2004), an extraordinarily high labeling efficiency (Reedy and Bullard, 1996). Moreover, the gold particles are associated directly with tip links and not randomly distributed around the epitopes as one would expect. Other studies have localized cadherin 23 in transient ankle links, but failed to detect immunolabeling of tip links (Lagziel et al., 2005; Michel et al., 2005; Rzadzinska et al., 2005). These data suggest a role for cadherin 23 in bundle maintenance rather than in mechanotransduction (Noben-Trauth et al., 2003; Holme and Steel, 2004).

The tip links that we have observed are of awkward dimensions to accommodate cadherin 23. The shorter links are too long for a cadherin 23 dimer and too short for a tetramer. If they include cadherin 23 tetramers, the longer links would require either a receptor molecule of 40-45 nm or an extensive region of filament pairing with doubled thickness (Tsuprun et al., 2004), which was not observed in our tomograms. Moreover, cadherin 23 is expected to be rigid in contrast to the tip link's tendency to curl up after loss of membrane contact.

Another candidate for the tip link is fibronectin, an abundant extracellular glycoprotein of 200-250 kDa. Fibronectin varies in length between 110 nm and 160 nm

(Erickson and Carrell, 1983), probably as a consequence of alternative mRNA splicing (Gorski et al., 1996; Zhao et al., 2001; Liu et al., 2003). Although purified fibronectin is vulnerable to a variety of proteases including subtilisin (Gold et al., 1979; Ruoslahti et al., 1979), conformational changes render it refractory to proteolysis (Ohashi et al., 1999). Fibronection occurs as a dimer that is connected by a C-terminal disulfide bridge, therefore rendering the molecule susceptible to reducing agents.

Fibronectin is very elastic, extending thrice its resting length owing to the unfolding of successive FN-III domains, each of which is predicted to open reversibly in response to small stretching forces (Erickson, 1994; Baneyx et al., 2002; Li et al., 2005). When broken, fibronectin fibrils relax to about one-third to one-quarter of their original length, suggesting that a globular conformation is most stable (Ohashi et al., 1999; Erickson, 2002). This behavior is consistent with the tendency of detached tip links to curl up.

Fibronectin typically binds integrin through the RGD motif of the FN-III 10 region, but it can also attach at its N-terminus (Pankov and Yamada, 2002) to lipid rafts containing the glycosphingolipid GM1 (Blum et al., 2005), which occurs in hair bundles (Santi et al., 1994). In addition, the N-terminal region can bind to the FN-III 12-14 domain, resulting in filament branching (Mao and Schwarzbauer, 2005).

Tip-link model

Our results suggest that each tip link comprises a dimer of fibronectin dimers that either reside side-by-side or are helically arranged, and that connect at their N-termini to the stereociliary surface. Auxiliary links connect to the FN-III 12-14 region of the fibronectin strands attached to the taller stereocilium, and possibly anchored by integrin molecules. This model implies that N-terminal but not other fragments of fibronectin

should interfere with the restoration of tip links after BAPTA treatment. Preliminary pharmacological data from zebrafish lateral-line neuromasts indicate that 30-kDa and 70-kDa N-terminal proteolytic fragments of fibronectin, but not a 45-kDa fragment, slow tip-link recovery (unpublished observation). Our model further suggests that proteins characteristic of fibronectin-integrin signaling should occur at the site of mechanotransduction. Fibronectin, Rho kinase, and FAK (Littlewood Evans and Muller, 2000) as well as talin (unpublished observation), have been detected in the hair bundle by immunolabeling. Despite its large size, the gene encoding fibronectin is unlikely to be identified as a cause of deafness, for knockout studies in mice indicate that the absence of fibronectin causes embryonic lethality.

Hair cells always reside in a pseudostratified epithelium, separated from the basal lamina by supporting cells. It is possible that the tip link and the associated molecules represent a focal adhesion complex that, in the absence of a basal lamina, is targeted to the apical cellular surface rather than to a typical basolateral site. When forced to confront the basal lamina owing to the absence of supporting cells, for example in *mind bomb* zebrafish mutants, hair cells degenerate (Haddon et al. 1999).

REFERENCES

Adato A, Lefevre G, Delprat B, Michel V, Michalski N, Chardenoux S, Weil D, El-Amraoui A, Petit C (2005) Usherin, the defective protein in Usher syndrome type IIA, is likely to be a component of interstereocilia ankle links in the inner ear sensory cells. Hum Mol Genet 14:3921-3932.

Assad JA, Shepherd GM, Corey DP (1991) Tip-link integrity and mechanical transduction in vertebrate hair cells. Neuron 7:985-994.

Auer M (2000) Three-dimensional electron cryo-microscopy as a powerful structural tool in molecular medicine. J Mol Med 78:191-202.

Bagger-Sjöbäck D (1974) The sensory hairs and their attachments in the lizard basilar papilla. Brain Behav Evol 10:88-94.

Bajaj C, Yu Z, Auer M (2003) Volumetric feature extraction and visualization of tomographic molecular imaging. J Struct Biol 144:132-143.

Baneyx G, Baugh L, Vogel V (2002) Fibronectin extension and unfolding within cell matrix fibrils controlled by cytoskeletal tension. Proc Natl Acad Sci USA 99:5139-5143.

Baugh L, Vogel V (2004) Structural changes of fibronectin adsorbed to model surfaces probed by fluorescence resonance energy transfer. J Biomed Mater Res A 69:525-534.

Blum S, Hug F, Hansch GM, Wagner C (2005) Fibronectin on activated T lymphocytes is bound to gangliosides and is present in detergent insoluble microdomains. Immunol Cell Biol 83:167-174.

Boeda B, El-Amraoui A, Bahloul A, Goodyear R, Daviet L, Blanchard S, Perfettini I, Fath KR, Shorte S, Reiners J, Houdusse A, Legrain P, Wolfrum U, Richardson G, Petit C (2002) Myosin VIIa, harmonin and cadherin 23, three Usher I gene products that cooperate to shape the sensory hair cell bundle. Embo J 21:6689-6699.

Braunfeld MB, Koster AJ, Sedat JW, Agard DA (1994) Cryo automated electron tomography: towards high-resolution reconstructions of plastic-embedded structures. J Microsc 174 (Pt 2):75-84.

Csukas SR, Rosenquist TH, Mulroy MJ (1987) Connections between stereocilia in auditory hair cells of the alligator lizard. Hear Res 30:147-155.

Di Palma F, Pellegrino R, Noben-Trauth K (2001) Genomic structure, alternative splice forms and normal and mutant alleles of cadherin 23 (Cdh23). Gene 281:31-41.

Erickson HP (1994) Reversible unfolding of fibronectin type III and immunoglobulin domains provides the structural basis for stretch and elasticity of titin and fibronectin. Proc Natl Acad Sci USA 91:10114-10118.

Erickson HP (2002) Stretching fibronectin. J Muscle Res Cell Motil 23:575-580.

Erickson HP, Carrell NA (1983) Fibronectin in extended and compact conformations. Electron microscopy and sedimentation analysis. J Biol Chem 258:14539-14544.

Erickson HP, Carrell N, McDonagh J (1981) Fibronectin molecule visualized in electron microscopy: a long, thin, flexible strand. J Cell Biol 91:673-678.

Fettiplace R, Hackney CM (2006) The sensory and motor roles of auditory hair cells. Nat Rev Neurosci 7:19-29.

Frangakis AS, Hegerl R (2001) Noise reduction in electron tomographic reconstructions using nonlinear anisotropic diffusion. J Struct Biol 135:239-250.

Frolenkov GI, Belyantseva IA, Friedman TB, Griffith AJ (2004) Genetic insights into the morphogenesis of inner ear hair cells. Nat Rev Genet 5:489-498.

Furness DN, Hackney CM (1985) Cross-links between stereocilia in the guinea pig cochlea. Hear Res 18:177-188.

Gillespie PG, Dumont RA, Kachar B (2005) Have we found the tip link, transduction channel, and gating spring of the hair cell? Curr Opin Neurobiol 15:389-396.

Gold LI, Garcia-Pardo A, Frangione B, Franklin EC, Pearlstein E (1979) Subtilisin and cyanogen bromide cleavage products of fibronectin that retain gelatin-binding activity. Proc Natl Acad Sci USA 76:4803-4807.

Goodyear R, Richardson G (1999) The ankle-link antigen: an epitope sensitive to calcium chelation associated with the hair-cell surface and the calycal processes of photoreceptors. J Neurosci 19:3761-3772.

Goodyear RJ, Richardson GP (2003) A novel antigen sensitive to calcium chelation that is associated with the tip links and kinocilial links of sensory hair bundles. J Neurosci 23:4878-4887.

Goodyear RJ, Marcotti W, Kros CJ, Richardson GP (2005) Development and properties of stereociliary link types in hair cells of the mouse cochlea. J Comp Neurol 485:75-85.

Goodyear RJ, McGee J, Weston MD, Legan PK, Bhattacharya G, Cosgrove D, McMillan DR, White PC, Walsh E, RIchardson GP (2006) Identification of the Ankle Link Antigen as the Usher 2c Protein, VLGR1, a Protein Required for Cochlear Hair Bundle Development. In: ARO 2006 Midwinter Meeting, Poster # 48.

Gorski GK, Aros MC, Norton PA (1996) Characterization of mouse fibronectin alternative mRNAs reveals an unusual isoform present transiently during liver development. Gene Expr 6:139-149.

He W, Cowin P, Stokes DL (2003) Untangling desmosomal knots with electron tomography. Science 302:109-113.

Hillman DE, Lewis ER (1971) Morphological basis for a mechanical linkage in otolithic receptor transduction it the frog. Science 174:416-419.

Holme RH, Steel KP (2002) Stereocilia defects in waltzer (Cdh23), shaker1 (Myo7a) and double waltzer/shaker1 mutant mice. Hear Res 169:13-23.

Holme RH, Steel KP (2004) Progressive hearing loss and increased susceptibility to noise-induced hearing loss in mice carrying a Cdh23 but not a Myo7a mutation. J Assoc Res Otolaryngol 5:66-79.

Horowitz RA, Giannasca PJ, Woodcock CL (1990) Ultrastructural preservation of nuclei and chromatin: improvement with low-temperature methods. J Microsc 157:205-224.

Hudspeth AJ (2005) How the ear's works work: mechanoelectrical transduction and amplification by hair cells. C R Biol 328:155-162.

Jacobs RA, Hudspeth AJ (1990) Ultrastructural correlates of mechanoelectrical transduction in hair cells of the bullfrog's internal ear. Cold Spring Harb Symp Quant Biol 55:547-561.

Jiang W, Baker ML, Wu Q, Bajaj C, Chiu W (2003) Applications of a bilateral denoising filter in biological electron microscopy. J Struct Biol 144:114-122.

Kachar B, Parakkal M, Kurc M, Zhao Y, Gillespie PG (2000) High-resolution structure of hair-cell tip links. Proc Natl Acad Sci USA 97:13336-13341.

Kussel-Andermann P, El-Amraoui A, Safieddine S, Nouaille S, Perfettini I, Lecuit M, Cossart P, Wolfrum U, Petit C (2000) Vezatin, a novel transmembrane protein, bridges myosin VIIA to the cadherin-catenins complex. Embo J 19:6020-6029.

Lagziel A, Ahmed ZM, Schultz JM, Morell RJ, Belyantseva IA, Friedman TB (2005) Spatiotemporal pattern and isoforms of cadherin 23 in wild type and waltzer mice during inner ear hair cell development. Dev Biol 280:295-306.

Li L, Huang HH, Badilla CL, Fernandez JM (2005) Mechanical unfolding intermediates observed by single-molecule force spectroscopy in a fibronectin type III module. J Mol Biol 345:817-826.

Littlewood Evans A, Muller U (2000) Stereocilia defects in the sensory hair cells of the inner ear in mice deficient in integrin alpha8beta1. Nat Genet 24:424-428.

Liu X, Zhao Q, Collodi P (2003) A truncated form of fibronectin is expressed in fish and mammals. Matrix Biol 22:393-396.

Mao Y, Schwarzbauer JE (2005) Fibronectin fibrillogenesis, a cell-mediated matrix assembly process. Matrix Biol 24:389-399.

McDonald K (1999) High-pressure freezing for preservation of high resolution fine structure and antigenicity for immunolabeling. Methods Mol Biol 117:77-97.

McMillan DR, White PC (2004) Loss of the transmembrane and cytoplasmic domains of the very large G-protein-coupled receptor-1 (VLGR1 or Mass1) causes audiogenic seizures in mice. Mol Cell Neurosci 26:322-329.

Michel V, Goodyear RJ, Weil D, Marcotti W, Perfettini I, Wolfrum U, Kros CJ, Richardson GP, Petit C (2005) Cadherin 23 is a component of the transient lateral links in the developing hair bundles of cochlear sensory cells. Dev Biol 280:281-294.

Mould AP, Garratt AN, Puzon-McLaughlin W, Takada Y, Humphries MJ (1998) Regulation of integrin function: evidence that bivalent-cation-induced conformational changes lead to the unmasking of ligand-binding sites within integrin alpha5 beta1. Biochem J 331 (Pt 3):821-828.

Nagar B, Overduin M, Ikura M, Rini JM (1996) Structural basis of calcium-induced E-cadherin rigidification and dimerization. Nature 380:360-364.

Neugebauer DC, Thurm U (1987) Surface charges of the membrane and cell adhesion substances determine the structural integrity of hair bundles from the inner ear fish. Cell Tissue Res 249:199-207.

Nicastro D, McIntosh JR, Baumeister W (2005) 3D structure of eukaryotic flagella in a quiescent state revealed by cryo-electron tomography. Proc Natl Acad Sci USA 102:15889-15894.

Noben-Trauth K, Zheng QY, Johnson KR (2003) Association of cadherin 23 with polygenic inheritance and genetic modification of sensorineural hearing loss. Nat Genet 35:21-23.

Ohashi T, Kiehart DP, Erickson HP (1999) Dynamics and elasticity of the fibronectin matrix in living cell culture visualized by fibronectin-green fluorescent protein. Proc Natl Acad Sci USA 96:2153-2158.

Osborne MP, Comis SD (1990) Action of elastase, collagenase and other enzymes upon linkages between stereocilia in the guinea-pig cochlea. Acta Otolaryngol 110:37-45.

Pankov R, Yamada KM (2002) Fibronectin at a glance. J Cell Sci 115:3861-3863.

Pettersen EF, Goddard TD, Huang CC, Couch GS, Greenblatt DM, Meng EC, Ferrin TE (2004) UCSF Chimera--a visualization system for exploratory research and analysis. J Comput Chem 25:1605-1612.

Pickles JO, Comis SD, Osborne MP (1984) Cross-links between stereocilia in the guinea pig organ of Corti, and their possible relation to sensory transduction. Hear Res 15:103-112.

Pickles JO, Brix J, Manley GA (1990) Influence of collagenase on tip links in hair cells of the chick basilar papilla. Hear Res 50:139-143.

Price TM, Rudee ML, Pierschbacher M, Ruoslahti E (1982) Structure of fibronectin and its fragments in electron microscopy. Eur J Biochem 129:359-363.

Reedy MC, Bullard B (1996) The Insect Flight Muscle Sarcomere as a Model System for Immunolocalization. Methods 10:219-233.

Robertson D, Monaghan P, Clarke C, Atherton AJ (1992) An appraisal of low-temperature embedding by progressive lowering of temperature into Lowicryl HM20 for immunocytochemical studies. J Microsc 168 (Pt 1):85-100.

Ruoslahti E, Hayman EG, Kuusela P, Shively JE, Engvall E (1979) Isolation of a tryptic fragment containing the collagen-binding site of plasma fibronectin. J Biol Chem 254:6054-6059.

Rzadzinska AK, Derr A, Kachar B, Noben-Trauth K (2005) Sustained cadherin 23 expression in young and adult cochlea of normal and hearing-impaired mice. Hear Res 208:114-121.

Santi PA, Mancini P, Barnes C (1994) Identification and localization of the GM1 ganglioside in the cochlea using thin-layer chromatography and cholera toxin. J Histochem Cytochem 42:705-716.

Sawaguchi A, McDonald KL, Forte JG (2004) High-pressure freezing of isolated gastric glands provides new insight into the fine structure and subcellular localization of H+/K+-ATPase in gastric parietal cells. J Histochem Cytochem 52:77-86.

Shapiro L, Fannon AM, Kwong PD, Thompson A, Lehmann MS, Grubel G, Legrand JF, Als-Nielsen J, Colman DR, Hendrickson WA (1995) Structural basis of cell-cell adhesion by cadherins. Nature 374:327-337.

Siemens J, Kazmierczak P, Reynolds A, Sticker M, Littlewood-Evans A, Muller U (2002) The Usher syndrome proteins cadherin 23 and harmonin form a complex by means of PDZ-domain interactions. Proc Natl Acad Sci USA 99:14946-14951.

Siemens J, Lillo C, Dumont RA, Reynolds A, Williams DS, Gillespie PG, Muller U (2004) Cadherin 23 is a component of the tip link in hair-cell stereocilia. Nature 428:950-955.

Small JV (1981) Organization of actin in the leading edge of cultured cells: influence of osmium tetroxide and dehydration on the ultrastructure of actin meshworks. J Cell Biol 91:695-705.

Sollner C, Rauch GJ, Siemens J, Geisler R, Schuster SC, Muller U, Nicolson T (2004) Mutations in cadherin 23 affect tip links in zebrafish sensory hair cells. Nature 428:955-959.

Sotomayor M, Corey DP, Schulten K (2005) In search of the hair-cell gating spring elastic properties of ankyrin and cadherin repeats. Structure 13:669-682.

Taylor KA, Schmitz H, Reedy MC, Goldman YE, Franzini-Armstrong C, Sasaki H, Tregear RT, Poole K, Lucaveche C, Edwards RJ, Chen LF, Winkler H, Reedy MK (1999) Tomographic 3D reconstruction of quick-frozen, Ca2+-activated contracting insect flight muscle. Cell 99:421-431.

Tomasini-Johansson BR, Annis DS, Mosher DF (2006) The N-terminal 70-kDa fragment of fibronectin binds to cell surface fibronectin assembly sites in the absence of intact fibronectin. Matrix Biol.

Tsuprun V, Santi P (2000) Helical structure of hair cell stereocilia tip links in the chinchilla cochlea. J Assoc Res Otolaryngol 1:224-231.

Tsuprun V, Goodyear RJ, Richardson GP (2004) The structure of tip links and kinocilial links in avian sensory hair bundles. Biophys J 87:4106-4112.

van Wijk E, van der Zwaag B, Peters T, Zimmermann U, Te Brinke H, Kersten FF, Marker T, Aller E, Hoefsloot LH, Cremers CW, Cremers FP, Wolfrum U, Knipper M, Roepman R, Kremer H (2006) The DFNB31 gene product whirlin connects to the Usher protein network in the cochlea and retina by direct association with USH2A and VLGR1. Hum Mol Genet 15:751-765.

Volkmann N (2002) A novel three-dimensional variant of the watershed transform for segmentation of electron density maps. J Struct Biol 138:123-129.

Volkmann N, DeRosier D, Matsudaira P, Hanein D (2001) An atomic model of actin filaments cross-linked by fimbrin and its implications for bundle assembly and function. J Cell Biol 153:947-956.

Zhao Q, Liu X, Collodi P (2001) Identification and characterization of a novel fibronectin in zebrafish. Exp Cell Res 268:211-219.

Zhao Y, Yamoah EN, Gillespie PG (1996) Regeneration of broken tip links and restoration of mechanical transduction in hair cells. Proc Natl Acad Sci USA 93:15469-15474.

	1	2		3		4	5	6	7	8	9	10	11	12	13	14	15
Figure	2a	2b		6		9F	9G	9H	9I	9J	-	-	9A	9B	9C	9D	9E
Intermembrane distance (nm)	100-250	100-250		100		115	119	105	117	110	117	140	168	140	168	168	168
Length (nm)	~125	~125		~115		115	-	105	117	110	117	-	168	-	-	168	168
Insertion angle (degrees)	30-90	30-90		70-90		52	28	37	34	27	37	35	28	37	33	21	31
Preparation	TX	TX		PLT		PLT	PLT	PLT	CP	CP	CP	PLT	PLT	PLT	PLT	TX	TX
Microscope	CM 200 FEG	CM 200 FEG		CM 200		CM 200	CM 200	CM 200	EM 430	EM 430	CM 200 FEG	CM 200	CM 200	CM 200	CM 200	CM 200 FEG	CM 200 FEG
Voxel (nm)	1.78	1.78		0.82		0.54	0.82	0.82	1.2	1.2	0.93	0.82	0.82	0.82	0.82	1.78	1.78
Range of tilt angles (degrees)	-47 +48	-47 +47		-75 +72		-69 +73	-74 +71	-75 +67	-48 +47	-48 +47	-42 50	-73 +72	-75 +69	-73 +71	-61 +71	-47 +48	-47 +48
Alignment error (pixel)	0.95	1.31		1.12		0.93	1.69	1.17	0.92	0.92	1.32	0.93	0.84	0.69	0.86	1.11	1.20

Table 1.   Data collection and analysis summary for basal links (1-2), kinociliary links (3), and tip links (4-15). PLT, Dehydration during progressive lowering of temperature; CP, conventional preparation with dehydration on ice; TX, Extraction with Triton X-100 followed by fixation and dehydration during progressive lowering of temperature.

FIGURE LEGENDS

Figure 1. *A*, A projection view of the basal tapers of two stereocilia in a 100-nm-thick section of a Triton X-100-treated hair bundle shows the basal links connecting adjacent stereociliary membranes. In this image as well as those of Figures 5 and 8, the colloidal-gold particles on the section's surface serve as fiducial markers for the alignment of images in the tilt series. *B*, A 1.7-nm slice through the three-dimensional reconstruction of the tomogram shows substantially more detail than does the projection image.

Figure 2. *A*, In these surface renderings of basal links from two data sets, a ball-and-stick model was interactively traced into the three-dimensional density maps to allow accurate length measurements. The longest filaments are about twice the length of the shortest. Some links interact side-by-side as dimers, whereas others may connect to a cell-surface receptor.

Figure 3. As a consequence of the stereociliary tapers, segmented basal links from two data sets extend distances ranging from 80 nm to 200 nm. Note that the filaments do not connect in the shortest possible way, but are instead curved or S-shaped; this behavior suggests a well-defined, rather stiff conformation of the basal-link protein.

Figure 4. Histograms display the lengths of different classes of hair-bundle link. *A*, Basal links show a very broad distribution of lengths suggestive of at least two structural classes. *B*, Kinociliary links are uniform in dimensions. *C*, Tip links fall into two well-defined length classes.

Figure 5. *A*, A projection view of the top of a hair bundle in a 100-nm-thick section displays the kinociliary links connecting the membrane of the kinocilium (right) with that of an adjacent stereocilium (left). *B*, A 0.82-nm slice through the three-dimensional reconstruction of the corresponding tomogram reveals the well-preserved actin lattice of the stereocilium and the periodic densities in the kinociliary membrane.

Figure 6. Kinociliary links represented by volume segmentation are clearly separated from one another and are either straight or slightly curved. Adjacent links occasionally lie too near one another to be resolved.

Figure 7. This surface rendering portrays the kinociliary links between the membranes of a stereocilium (left) and a kinocilium (right). Although the links appear interwound in projection images, progressive rotation of the reconstruction reveals their separation.

Figure 8. *A*, A projection view of a 100-nm-thick section of a hair bundle's beveled upper edge shows the tip link connecting the top of one stereocilium with the side of a longer adjacent stereocilium. *B*, A 0.82-nm thin slice through the three-dimensional reconstruction of the tomogram demonstrates that the tip link is intact and that the membrane of the shorter stereocilium displays tenting. *C*, A projection view of a second specimen shows a well-ordered actin array in the stereociliary cytoskeletons. *D*, A 0.82-nm slice through the reconstruction discloses that the tip link is detached from its lower insertion and somewhat curled. Note the tightly coiled densities adjacent to the upper insertions of both tip links.

Figure 9. In a gallery of tip links from ten of the 12 data sets, each link is shown in three different orientations defined by successive rotations of 45°. For each triplet, the

view on the right shows the tip link as projected onto the plane of the longer stereocilium's membrane surface. Roughly equal numbers of long and short tip links were encountered.

Figure 10. These higher-magnification views of the best-preserved tip link include a molecular model interactively traced into the three-dimensional density. At the left is a view of the link in the orientation typically observed in sectioned hair bundles. The second image shows the result of rotation by 45°; the third image reflects both a rotation of 90° and a tilt of 28° to place the reconstruction in the plane of the figure. The fourth image show an interactively traced model within the tip link; the final three images show the model in the same orientation and after rotations of 45° and 90°.

Figure 11. *A*, This surface rendering depicts a segmented tip link interconnecting two stereociliary membranes. The main tip link is shown in gold, two strands connecting to the tip link and membrane are rendered in purple, and a membrane-anchored structure is displayed in red. *B*, The same link is depicted after a rotation of 90°. *C*, In a higher-magnification view of the link's upper insertion, the lower component of a bilobed feature is shown in maroon and the upper constituent in green. *D*, Another surface rendering displays a broken tip link. *E* and *F*, Successively higher-magnification views emphasize the auxiliary link, colored maroon, at the main link's upper end. *G*, Another structure, possibly a broken tip link, resides 150 nm above the tip link's insertion. **[Scale bars = 20 nm]**

SUPPLEMENTARY FIGURE LEGENDS

Figure S1.   Influence of sample preparation on ultrastructural preservation. Upper left panel: Conventional preparation resulting in poorly preserved actin filaments. Upper right and lower left panel: actin filaments are well-preserved by OIP preparation but extraction visible in distal region of stereocilia. Note that in the upper right panel all actin filaments are nulceated at the same height. Lower right panel: Omission of tannic acid in the primary fixative of the OIP regiments leads to increased membrane articfacts.

Figure S2.   High pressure frozen, freeze-substituted frog sacculus hair cell stereocilia: Left panel: Overview of one of very few well-preserved hair bundles. Note that the bundle appears in side view above and in cross section below an apparent otholithic membrane rupture, indicating substantial mechanical forces during freezing. Middle panel and right panel: Stereocilia preserved by high-pressure freezing display a smooth membrane surface.

Figure S3.   Model of fimbrin cross-linked actin bundle containing 5 actin filaments in a 12 nm hexagonal spacing fits nicely into the density map of stereocilia actin bundle, suggesting that no detectable shrinkage of the sample occurred.

Figure S4.   Analysis of eight kinociliary link shows that all links display a similar profile, suggesting a filament thickness of 4-5nm. Bilateral filtering slightly increases filemant thickness (data not shown).

Figure S5.   Wire-frame surface rendering of cell surface anchor of auxiliary link of Fig. 8a and 11a, with an atomic model of an integrin extracellular domain superimposed on

the density map. The fit is remarkably good given the limited resolution of EM tomography. More recent results indicate that the alpha and beta integrin domains are not as closely packed, hence, which would even better fit the density obtained by EM tomography.
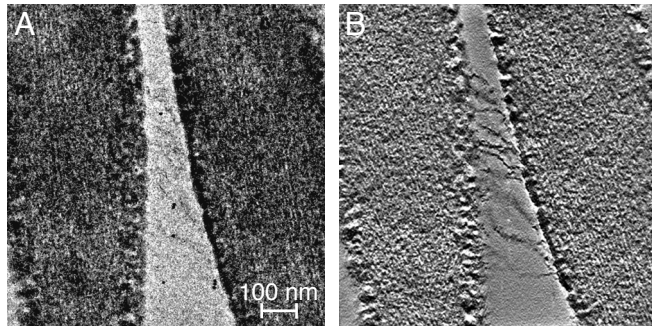
100 nm

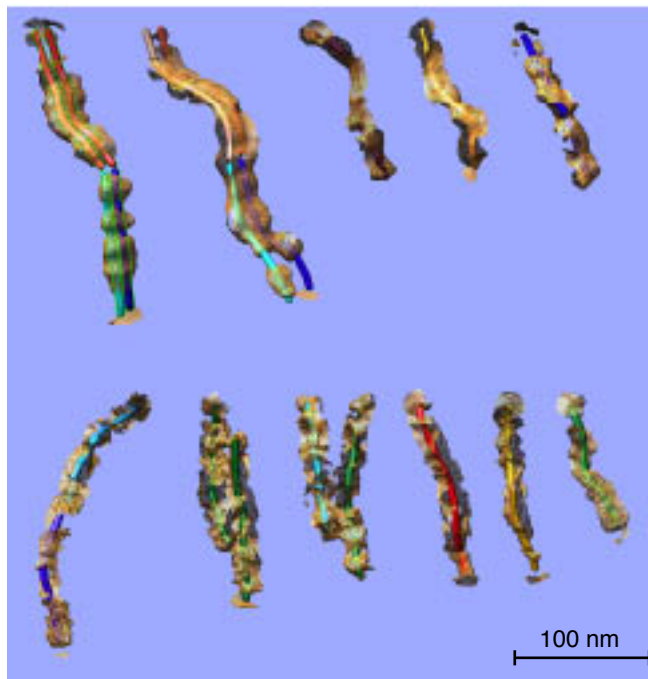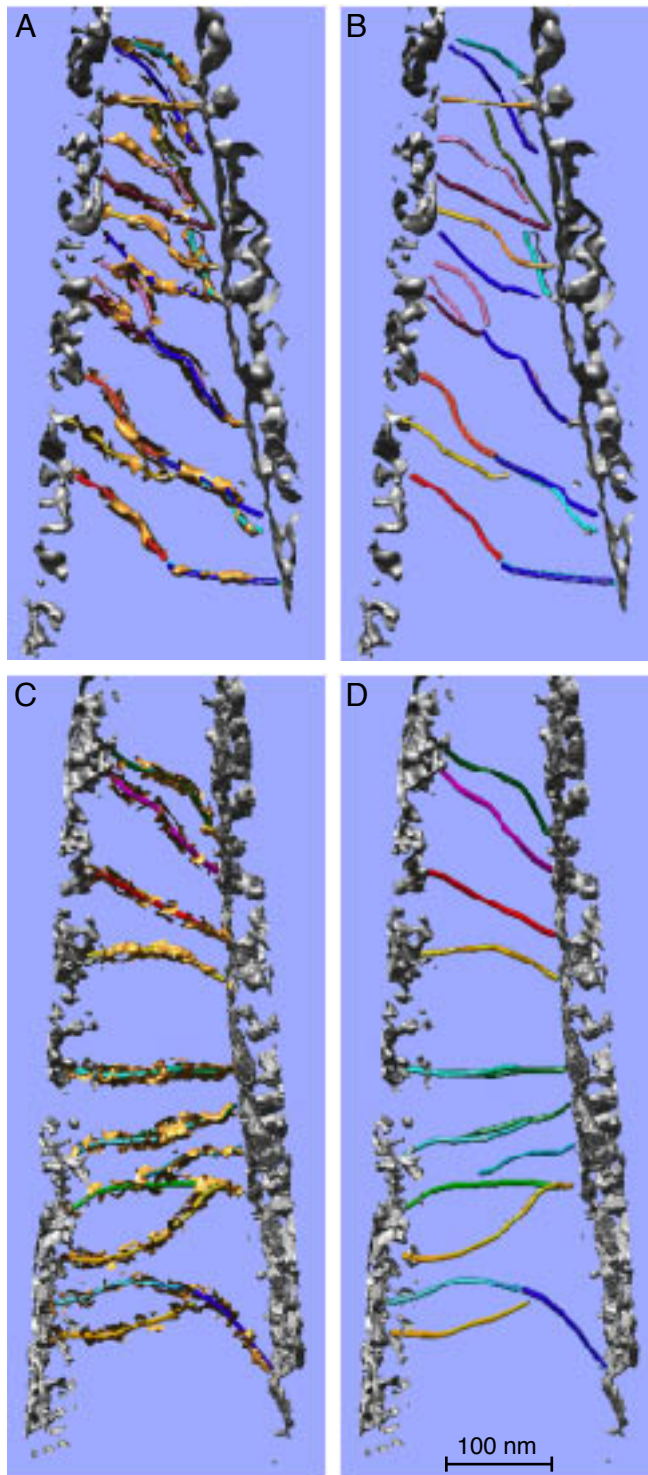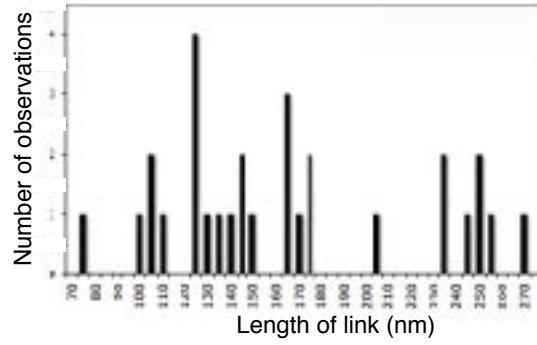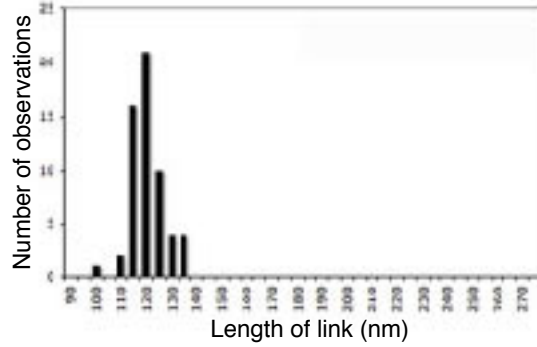Figure 1

100 nm

Figure 2
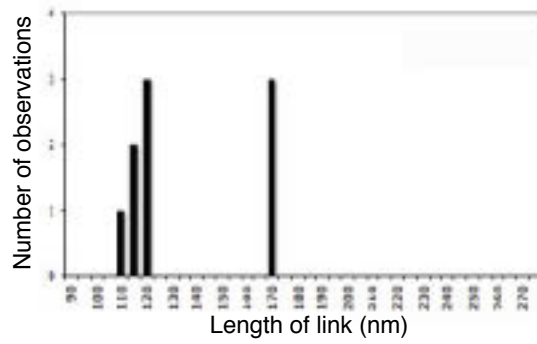
100 nm

Figure 3

A: Basal links

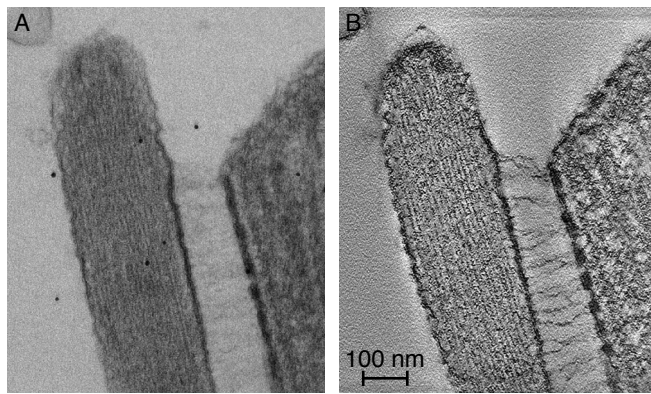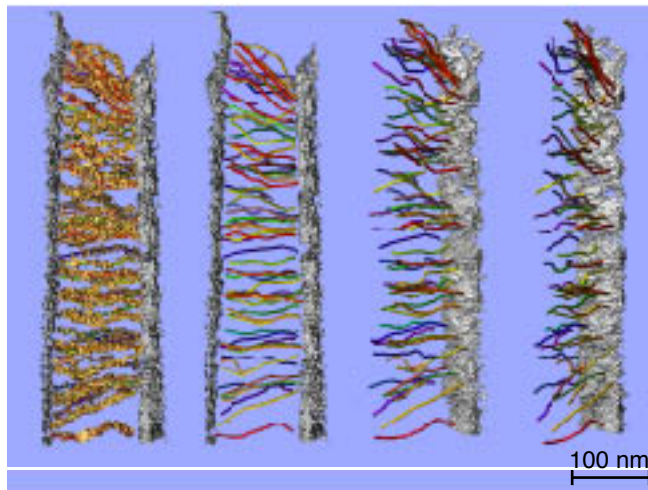## B: Kinociliary links

C: Tip links

Figure 4

Figure 5

100 nm

Figure 6

100 nm

Figure 7

Figure 8

100 nm

Figure 9

20 nm

Figure 10

Figure 11